Heavy-atom engineering of thermally activated delayed fluorophores for high-performance X-ray imaging scintillators

Heavy-Atom Engineering of Thermally Activated Delayed Fluorophores for High-Performance X-ray Imaging Scintillators

Jian-Xin Wang,[1] Luis Gutiérrez-Arzaluz,[1,2#] Xiaojia Wang,[3#] Tengyue He,[1] Yuhai Zhang,[3] Mohamed Eddaoudi,[1] Osman M. Bakr,[2] and Omar F. Mohammed*[1]

[1]Advanced Membranes and Porous Materials Center, Division of Physical Science and Engineering, King Abdullah University of Science and Technology, Thuwal 23955-6900, Kingdom of Saudi Arabia

[2]KAUST Catalysis Center, Division of Physical Sciences and Engineering, King Abdullah University of Science and Technology, Thuwal 23955-6900, Kingdom of Saudi Arabia

[3]Institute for Advanced Interdisciplinary Research (iAIR), University of Jinan, Jinan 250022, Shandong China

[#]These authors contributed equally to this work

Correspondence: omar.abdelsaboor@kaust.edu.sa

Abstract: The architectural design and fabrication of low-cost and reliable organic X-ray imaging scintillators with high light yield, ultralow detection limits, and excellent imaging resolution is becoming one of the most attractive research directions for chemists, materials scientists, physicists, and engineers due to the devices' promising scientific and applied technological implications. However, the optimal balance between the X-ray absorption capability, exciton utilization efficiency, and photoluminescence quantum yield (PLQY) of organic scintillation materials is extremely difficult to achieve because of several competitive nonradiative processes, including intersystem crossing and internal conversion. Here, we introduced heavy atoms (Cl, Br, I) into thermally activated delayed fluorescence (TADF) chromophores to significantly increase their X-ray absorption cross-section while maintaining their unique TADF properties and high PLQY. Most importantly, the X-ray imaging screens fabricated using TADF-Br chromophores exhibited a relative light yield of approximately 20,000 photons/MeV, which is comparable with some inorganic scintillators. In addition, the detection limit of 64.5 nGy s^{-1} is several times lower than the standard dosage for X-ray diagnostics, demonstrating its high potential in medical radiography. Moreover, a high X-ray imaging resolution of 18.3 line pairs (lp) mm^{-1} was successfully achieved, exceeding the resolution of all the reported organic scintillators and most conventional inorganic scintillators. This study could help revive research on organic X-ray imaging scintillators and pave the way toward exciting applications for radiology and security screening.

Introduction

Scintillators, which convert ionizing radiation into visible photons, have received much attention in recent years due to their applications in science and daily life, including radiation detection, high-energy physics, medical radiography, security screening, and astronomical discovery.[1-7] Currently, high-performance X-ray imaging scintillators are fabricated almost exclusively from ceramic and perovskite materials, which themselves are typically fabricated under very harsh conditions or exhibit very poor air and light stability along with high environmental toxicity.[8-14] In contrast, organic scintillators exhibit inherent advantages, such as abundant resources, high mechanical flexibility, easy processing, low cost, and large-area fabrication.[15-17] However, the low X-ray absorption cross-section and subsequently poor detection sensitivity of organic scintillators due to their limited effective atomic number (as X-ray absorption increases exponentially with atomic number) and inefficient exciton utilization efficiency have significantly impeded their evolution and possible commercialization.[18-20] Therefore, the exploration of new photoactive organic materials with outstanding scintillation performance is a promising research direction, as such materials are urgently needed.

X-ray photons generally interact with the heavy atoms in organic chromophores by the Compton effect, which generates scattering photons. By electron-electron scattering and Auger processes, a tremendous number of secondary electrons are produced, generating electron-hole pairs.[7] Singlet and triplet excitons are then generated according to the recombination of the electron-hole pairs in a 1:3 ratio.[17,19,21] In this case, the light emission of commonly used organic fluorescent chromophores is controlled by the selection rules for electric dipoles. The few allowed transitions from singlet-excited to singlet-ground states waste many triplet excitons, leading to only 25% exciton utilization efficiency.[19] The introduction of heavy atoms (Br, I) into fluorescent emitters could greatly increase X-ray absorption and provide an opportunity to transition from fluorescence to phosphorescence by the heavy atom effect, which would further increase the overall exciton utilization efficiency from 25% through fluorescence to 75% through phosphorescence.[22] However, the photoluminescence quantum yield (PLQY) of organic phosphorescent materials is much lower than the fluorescence, and their phosphorescence is easily quenched by oxygen, which highly limits their radioluminescence (RL) efficiency.[23-25] Thermally activated delayed fluorescence (TADF) chromophores, in contrast, are some of the best candidates (if not the best) for high-performance scintillators due to their minimized singlet-triplet energy gap. This minimized gap allows such chromophores to harness both singlet and triplet excitons for light emission through highly efficient spin upconversion from triplet states to radiative singlet states, leading to unit exciton utilization efficiency (Figure 1a).[26-31] However, introducing heavy atoms into TADF chromophores could also quench their luminescence or induce phosphorescence owing to the heavy atom effect. Therefore, the search for a suitable TADF system and appropriate molecular engineering approach to retain TADF performance after the introduction of heavy atoms, as a way of generating new high-performance organic scintillators, is of great interest to materials scientists, chemists, and engineers.

In this study, we carefully addressed this challenge by introducing heavy atoms (Cl, Br, I) into a TADF chromophore in which the highest occupied molecular orbital (HOMO) and lowest unoccupied molecular orbital (LUMO) are well separated. The TADF properties and PLQY were not influenced by the introduction of heavy atoms, as evidenced by steady-state and ultrafast time-resolved experiments and density functional theory (DFT) calculations. More importantly, the X-ray imaging screens created using TADF-Br chromophore exhibited a relative light yield of approximately 20,000 photons/MeV, which is 5 times higher than that of the best TADF scintillator reported recently (the highest relative light yield among reported TADF scintillators is 3700 photons/MeV[15] according to the calculation method provided in this article).[15,19,32,33] In addition, the detection limit of 64.5 nGy s^{-1} obtained for the TADF-Br film is several times lower than the standard dosage for X-ray diagnostics (5.5 μGy s^{-1})[1]. Moreover, a high X-ray imaging resolution of 18.3 lp mm^{-1}

can be achieved, exceeding all the reported organic and most conventional inorganic scintillators.[10,34-39] These findings provide a powerful design approach and promising new alternative materials for fabricating organic X-ray imaging scintillators with outstanding sensitivity, low cost, and high stability using a simple molecular engineering strategy involving TADF chromophores.

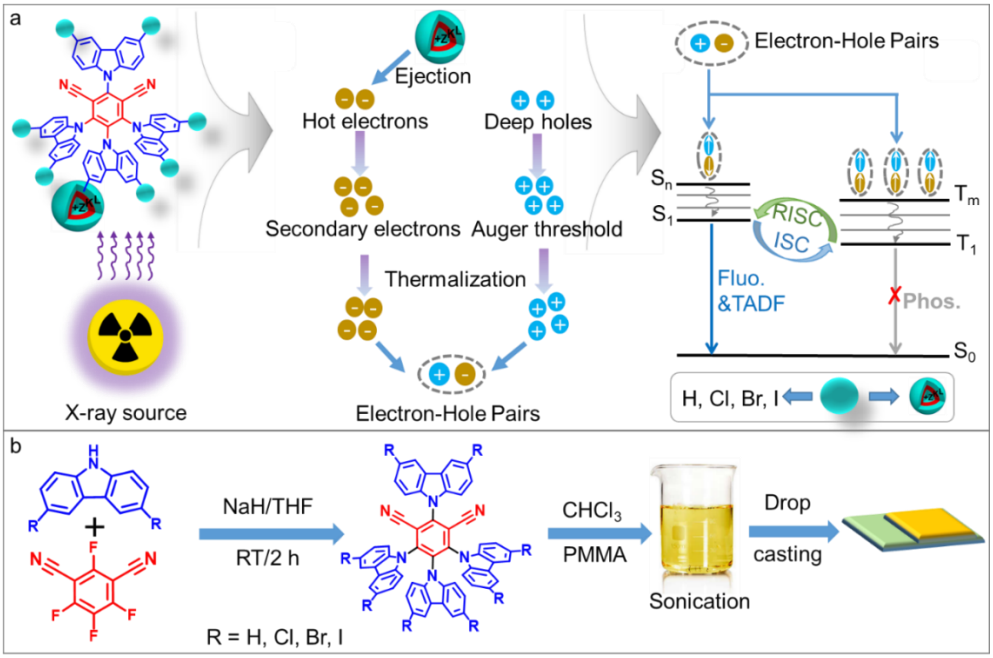

Figure 1. (a) Mechanism by which the radioluminescence efficiency of TADF scintillators is significantly enhanced, which occurs due to the enhanced X-ray absorption of heavy elements and their unit exciton utilization efficiency. (b) One-step synthesis of TADF chromophores (TADF-H, TADF-Cl, TADF-Br, and TADF-I) and the corresponding method for fabricating X-ray imaging screens. ISC, intersystem crossing; RISC, reverse intersystem crossing; S, singlet; T, triplet; Fluo., fluorescence; Phos., phosphorescence; TADF, thermally activated delayed fluorescence.

TADF-H was selected as the preferred TADF system due to its large HOMO-LUMO separation, which largely minimizes the impact of heavy atoms on its TADF performance.[40,41] TADF-H can be synthesized by a one-pot method with a high reaction yield, and TADF-Cl, TADF-Br, and TADF-I can be easily obtained under the same reaction conditions by using different halogen-substituted carbazole reactants (Figure 1b). Due to the good processability of these TADF chromophores, the corresponding films, which can be used for radioluminescence and ultrafast spectroscopic measurements, as well as X-ray imaging screens, can be easily fabricated according to the methods illustrated in Figure 1b.

When doped into a polymethyl methacrylate (PMMA) matrix at 1 wt%, the four abovementioned TADF chromophores (TADF-H, TADF-Cl, TADF-Br, TADF-I) showed similar absorption bands over the ultraviolet and blue spectral ranges. The absorption spectra over the ranges of 320-350 nm and 370-390 nm are attributed to the π–π^* band of the carbazole derivative units and the localized charge transfer state, respectively. The shoulder peak above 400 nm is due to the delocalized charge transfer state, as previously reported (Figure 2a).[41] In contrast, the steady-state photoluminescence (PL) spectra of these TADF chromophores show a broad emission band from 450 to 650 nm centered at approximately 505 nm. Notably, the overlap between the absorption and emission spectra is quite small (free reabsorption feature); such minimal overlap is a prerequisite for high-performance scintillators. As expected, the delayed fluorescence lifetime

gradually decreased from 4.53 μs for the TADF-H chromophore to 1.42 μs for the TADF-I chromophore due to the heavy-atom-enhanced reverse intersystem crossing process (RISC) (Figures 2b and 2c). To more accurately ascertain the changes in the prompt fluorescence decay, we recorded the transient PL decay profiles for each TADF chromophore over a relatively short time window (Figure S1). The short fluorescence lifetime was also decreased from 5.63 ns to 0.21 ns (Figure 2d), which further confirmed the effects of the inner heavy atoms on the intersystem crossing (ISC) process, which accelerate both the prompt and delayed fluorescence processes. Notably, the introduction of heavy atoms in these TADF systems simultaneously accelerated the ISC and RISC processes, which are involved in the delayed fluorescence process rather than completely non-radiative transitions. In other words, while the heavy atoms may increase the non-radiative transitions, their delayed fluorescence is also enhanced leading to the maintenance of PLQY with the addition of halogens.

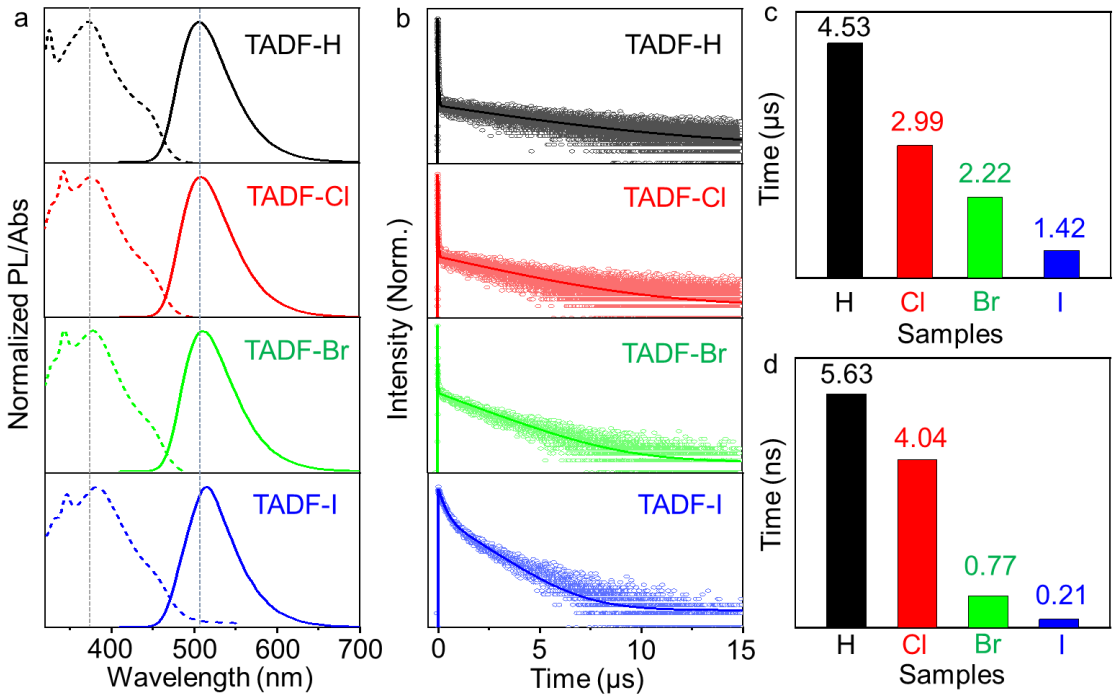

Figure 2. (a) Normalized absorption and emission spectra, (b) emission decay profiles of the TADF chromophores with different halogen substitutions (H: TADF-H, Cl: TADF-Cl, Br: TADF-Br, and I: TADF-I) doped into a polymethyl methacrylate (PMMA) matrix at 1 wt%, and (c-d) the corresponding fitted lifetimes over the long and short time ranges, respectively.

In addition, through density functional theory (DFT) calculations and its time-dependent variant (TD-DFT), we found that the HOMO was consistently localized on the carbazole units. The LUMO, meanwhile, resided on the isophthalonitrile moiety of these four TADF chromophores, indicating that the spatial separation between the HOMO and LUMO was not disturbed by the substitution of heavy atoms such as Br and I for H atoms (Figure 3a). We then turned our attention to the detailed behavior and mechanism of the delayed fluorescence of these TADF chromophores. Figure 3b shows the calculated spin-orbit coupling matrix element (SOCME) in the optimized S_1 geometry. The increase in atomic number can be associated with an increase in the SOCME values. These results suggest that the fast spin-flip process is more likely to occur in TADF-Br and TADF-I chromophores with heavy atoms, supporting the previous time-resolved photoluminescence measurements.

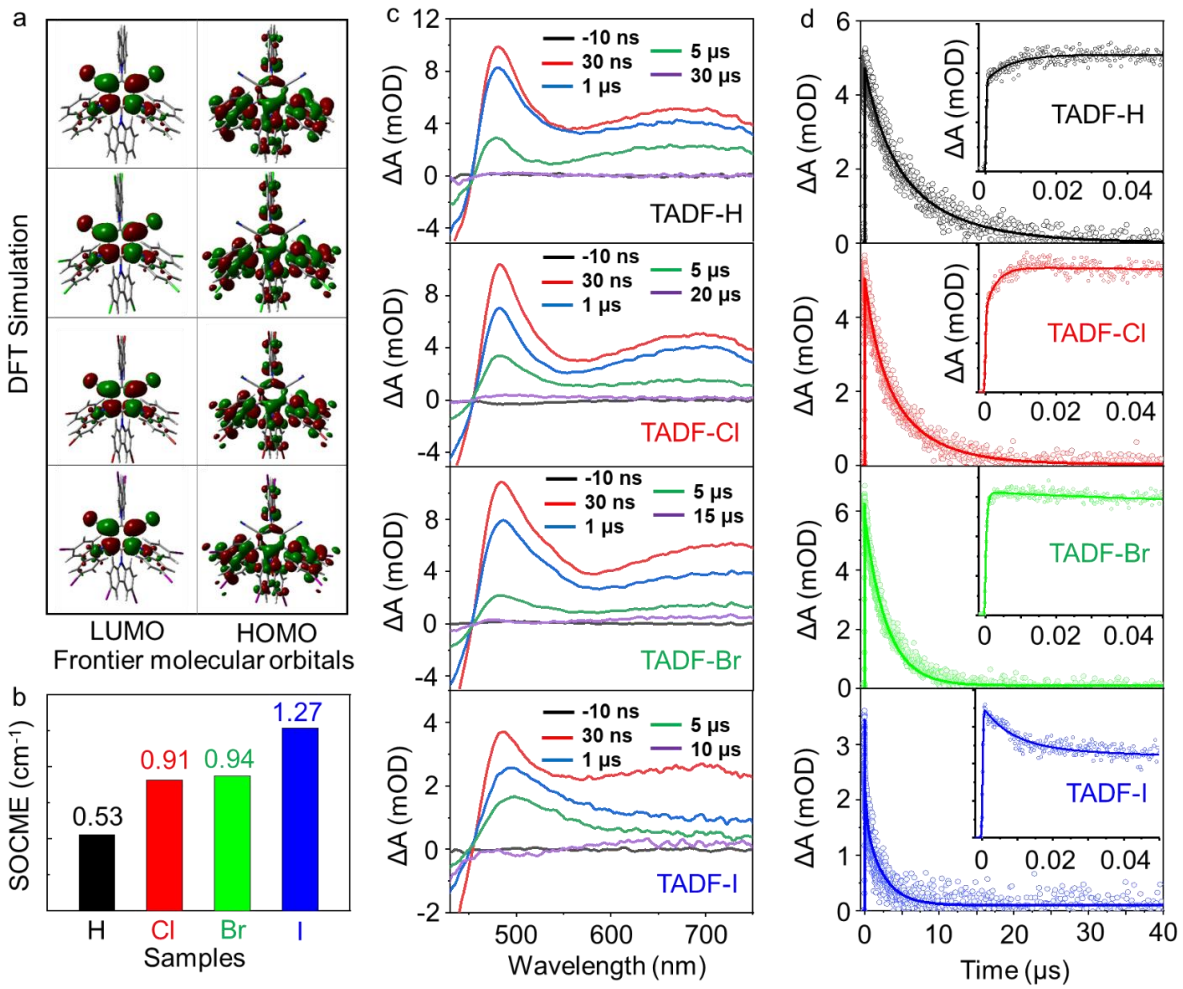

Figure 3. (a) Optimized structures and HOMO/ LUMO orbitals, and (b) calculated spin-orbit coupling matrix element (SOCME) of TADF-H, TADF-Cl, TADF-Br, and TADF-I chromophores. (c) Transient absorption spectra of TADF-H, TADF-Cl, TADF-Br, and TADF-I doped into a PMMA matrix at 1 wt%, with excitation at 400 nm at different delay times, and (d) the corresponding kinetic traces recorded at 710 nm (insets are the kinetic traces over short time ranges).

To further elucidate the influence of the heavy atoms on the delayed fluorescence of the TADF chromophores, their excited-state dynamics were investigated by nanosecond transient absorption (ns-TA) pump-probe spectroscopy. All of the TADF chromophores showed similar excited-state absorption bands due to their similar molecular structures. Immediately after photoexcitation of the TADF chromophores at 400 nm (Figure 3c), a negative band below 400 nm was observed and assigned to ground-state bleaching, while a broad positive band from 450 to 750 nm was attributed to photoinduced excited-state absorption. The singlet and triplet excited-state absorptions of these four TADF chromophores are highly encompassed due to their similar energy levels. After photoexcitation, the amplitude of the whole absorption band increased rapidly and then gradually decreased at longer delay times. It is worth noting that the decay of the excited states gradually accelerated when the heavy atom was changed from H to I, which is consistent with the heavy atom effect.

To clarify the dynamic relaxation mechanism of these TADF chromophores, the kinetic traces of each TADF chromophore were recorded at 710 nm (Figure 3d). The decay of the excited-state absorption became faster as the

atomic number was gradually increased (from H to I). The triplet excited-state lifetime decreased from 4.99 μs for the TADF-H chromophore to 1.21 μs for the TADF-I chromophore (Table S1); these data agreed well with the delayed fluorescence lifetime obtained from time-correlated single-photon counting (TCSPC) measurements. In addition, the rising components observed over the shorter time range also exhibited trends similar to those of the decay traces as the atomic number was gradually increased. This observation could be attributed to the intersystem crossing from the singlet excited state to the triplet excited state.

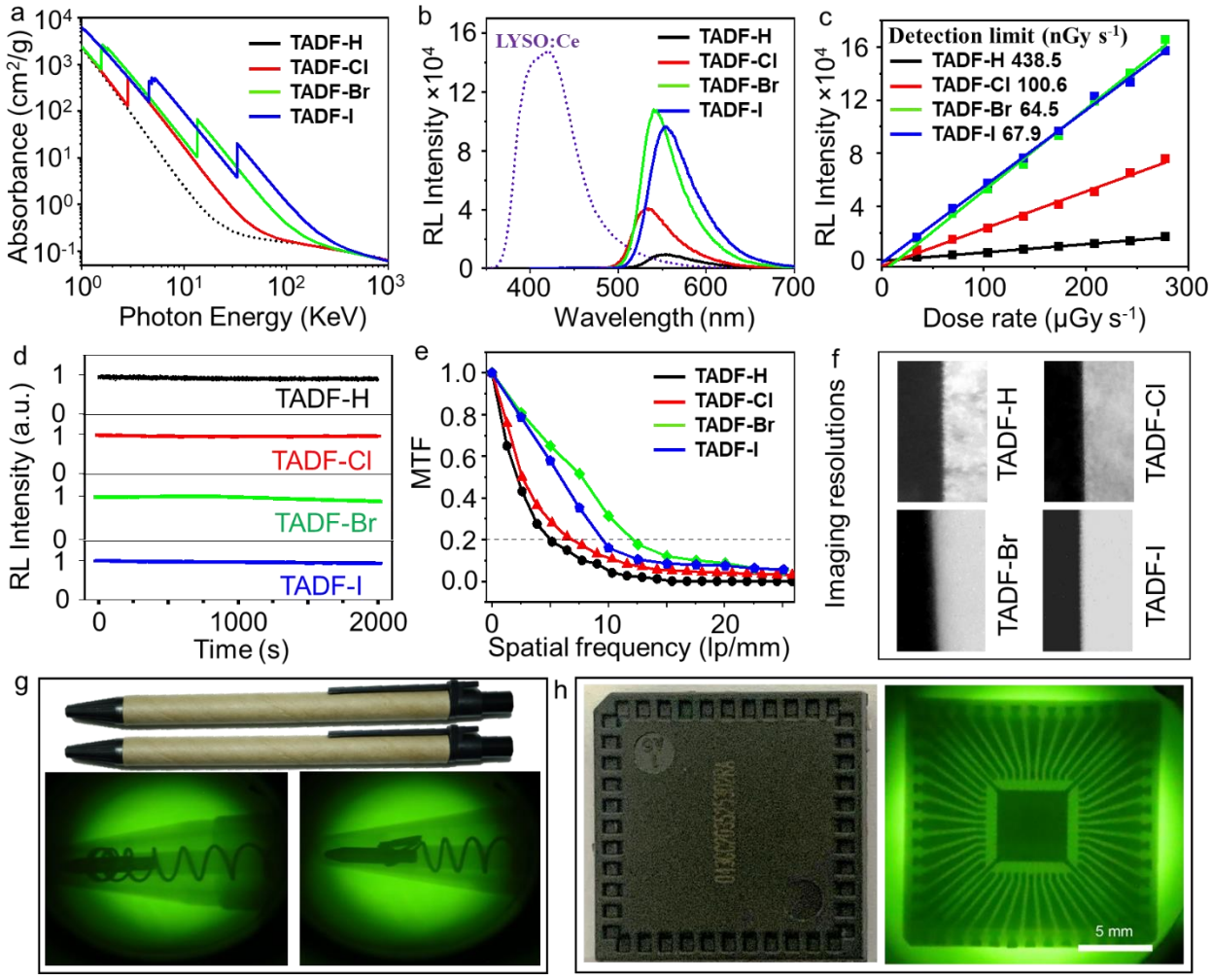

Figure 4. (a) X-ray absorption spectra of TADF-H, TADF-Cl, TADF-Br, and TADF-I chromophores measured as a function of X-ray energy.[42] (b) RL spectra of these four TADF chromophores (at the optimal thickness: TADF-H (0.5 mm), TADF-Cl (0.2 mm), TADF-Br (0.2 mm), and TADF-I (0.4 mm)) compared to the reference scintillator, LYSO:Ce. The relative light yield was calculated by integrating these X-ray-induced RL spectra and comparing the results with those obtained for the reference LYSO:Ce (dose rate, 174 μGy s^{-1}). (c) The detection limits of the TADF-H, TADF-Cl, TADF-Br, and TADF-I chromophores. (d) Normalized RL intensity at the corresponding emission maxima of these four TADF chromophore films under continuous X-ray irradiation (dose rate, 174 μGy s^{-1}). (e) Modulation transfer functions (MTFs) of the X-ray images for each TADF chromophore and (f) the corresponding X-ray edge images. Bright- and dark-field photographs of (g) pens and (h) an electronic chip before and after X-ray exposure (dose rate, 174 μGy s^{-1}).

To balance the performance of the TADF chromophores and the good processability of the scintillation films for X-ray imaging, we doped 60 wt% of each TADF chromophore into a PMMA matrix to prepare corresponding films with different thicknesses for X-ray correlated measurements (Figure S2 and Table S2). X-ray absorption measurements of these four TADF chromophores were first performed to investigate their X-ray absorption ability. As expected, the resonant absorption edges gradually increased from <0.5 KeV for the TADF-H chromophore to 33.2 KeV for the TADF-I chromophore, which confirmed the heavy atom effect on the X-ray photon absorption ability of the organic chromophores (Figure 4a).

According to the X-ray excited RL spectra, the RL intensity of each TADF chromophore with optimal thickness (Figure S3) gradually increased. A comparison with standard scintillators showed that these TADF chromophores exhibited highly increased relative light yields ranging from 1892 and 7076 photons/MeV for the TADF-H and TADF-Cl chromophores to 17691 and 18115 photons/MeV for the TADF-Br and TADF-I chromophores (dose rate, 174 μGy s^{-1}) (Figure 4b), respectively. The high relative light yield of the TADF-Br and TADF-I chromophores was mainly due to their higher X-ray absorption cross-section compared to TADF-H and TADF-Cl, as well as their unit exciton utilization efficiency and good PLQY (Table S3). Because the detection limit ultimately determines the minimum dosage required for detection and imaging, dose rate-dependent RL spectra were obtained for each TADF. The RL intensities of all the TADF chromophores were linearly correlated with the dosages (dose rate, 34.8 - 278 μGy s^{-1}) of the X-rays (Figures S4). The detection limit greatly improved from 438.5 and 100.6 nGy s^{-1} for TADF-H and TADF-Cl to 64.5 and 67.9 nGy s^{-1} for TADF-Br and TADF-I (Figures 4c and S5), respectively. The detection limit obtained for the TADF-Br chromophore was comparable to that of the commercial standard scintillator (LYSO:Ce) (Figure S6) and is approximately 92 times lower than the standard dosage for X-ray diagnostics (5.5 μGy s^{-1}),[1] demonstrating the material's high potential for X-ray imaging applications. In addition, all TADF chromophores exhibited good photostability; specifically, the RL intensity remained close to 100% under ionizing radiation with a dose rate of 174 μGy s^{-1} applied continuously for 2000 seconds (Figure 4d), highlighting the outstanding photostability of these TADF systems.

Inspired by the promising X-ray excited luminescence properties of these TADF chromophores, we characterized the imaging resolutions of four TADF films, as shown in Figure 4e. The X-ray imaging resolution also followed the trends exhibited by the RL intensity, and a high resolution of 12.0 lp mm^{-1} (at a modulation transfer function (MTF) = 0.2) was obtained for the TADF-Br scintillation screen, according to the MTF calculation of standard X-ray edge images (Figure 4f and Table S4). Such high imaging resolution exceeds that of most reported organic and inorganic materials, which further supports the high practical potential of this molecular engineering strategy for incorporating TADF chromophores into high-performance X-ray imaging scintillators. Furthermore, we performed a series of imaging tests using these TADF scintillators to demonstrate their practical value. Pens equipped with springs in different states were placed between an X-ray source and the TADF-Br films. The outline of this otherwise invisible spring was clearly presented on each film, while the plastic case was nearly transparent (Figure 4g). In addition, the application of this principle of X-ray contrast imaging also enabled the inspection of the complex inner structure of an electronic chip that is otherwise completely opaque to visible light. The complex structure of the electronic chip was clearly visualized using a TADF-Br scintillator screen (Figure 4h, (dose rate, 174 μGy s^{-1}, and the imaging photographs for the other TADF chromophores are shown in Figure S7).

To further investigate the potential of the heavy-atom engineered TADF materials in X-ray imaging application, we adjusted the doping ratio of TADF-Br to prepare a transparent screen (Figure S8a), achieving a high spatial resolution of 18.3 lp/mm. This ultrahigh resolution exceeded that of all the reported organic scintillators and most conventional

inorganic scintillators like LYSO:Ce, CsI, and $CsPbBr_3$ materials as shown in Figure S8b-c. More importantly, the transparent nature of the TADF-Br screen is amenable to high-resolution biological imaging. As shown in Figure S8d, the skeletons of the fish were clearly observed under X-ray exposure, further demonstrating the promising potential of the heavy-atom engineered TADF scintillator in medical radiography.

CONCLUSION

We developed a novel molecular engineering strategy for chemically modifying TADF chromophores with heavy atoms, which significantly enhanced the X-ray absorption cross-section of the chromophores while preserving their TADF properties. The excited-state dynamics of the TADF chromophores (TADF-H, TADF-Cl, TADF-Br, and TADF-I) were explored using steady-state and ultrafast time-resolved spectroscopy and DFT calculations. The high X-ray absorption cross-section, 100% exciton utilization efficiency, and the excellent PLQY of the heavy-atom engineered TADF scintillator lead to the highly improved scintillation performance, including a low detection limit of 64.5 nGy/s and high relative light yield (RL brightness) of ~ 20,000 photons/MeV, which is comparable (if not better) to perovskite nanosheets and nanocrystals. In addition, a transparent screen can be obtained by adjusting the doping ratio to further improve the X-ray imaging resolution of TADF-Br to 18.3 lp/mm, exceeding the resolution of all the reported organic scintillators and most conventional inorganic and commercial scintillators like LYSO:Ce, CsI, and $CsPbBr_3$ materials. We believe that our findings will serve as a benchmark for the fabrication of efficient organic scintillators in real-life applications, including medical and security screening from materials beyond high-cost ceramic crystals and perovskites by using a simple molecular engineering strategy on TADF chromophores.

ACKNOWLEDGMENTS

This work was supported by the King Abdullah University of Science and Technology (KAUST).

AUTHOR CONTRIBUTIONS

J.X.W. and O.F.M. conceived the project. J.X.W. synthesized the TADF chromophores, prepared all the films for measurements and applications, performed the steady-state experiments and some time-resolved experiments, and analyzed all the data. L.G.A. performed the TA and TCSPC measurements and the DFT calculations. X.W. and Y.H.Z. performed and analyzed the scintillation measurements. T.H. synthesized the $CsPbBr_3$ nanosheet. O.M.B and M.E. contributed to the discussion of the experimental data and provided valuable suggestions. O.F.M. supervised the project and suggested the analysis of the experimental data. J.X.W. and O.F.M. co-wrote the manuscript.

DECLARATION OF INTERESTS

The authors declare no competing interests.

REFERENCES

1 Chen, Q. *et al.* All-Inorganic Perovskite Nanocrystal Scintillators. *Nature.* **561**, 88-93 (2018).

2 Yu, D. *et al.* Two-Dimensional Halide Perovskite as Beta-Ray Scintillator for Nuclear Radiation Monitoring. *Nat. Commun.* **11**, 3395 (2020).

3 Wu, H., Ge, Y., Niu, G. & Tang, J. Metal Halide Perovskites for X-Ray Detection and Imaging. *Matter.* **4**, 144-163 (2021).

4 Liang, S. *et al.* Recent Advances in Synthesis, Properties, and Applications of Metal Halide Perovskite Nanocrystals/Polymer Nanocomposites. *Adv. Mater.* **33**, e2005888 (2021).

5 Heo, J. H. *et al.* High-Performance Next-Generation Perovskite Nanocrystal Scintillator for Nondestructive X-Ray Imaging. *Adv. Mater.* **31**, e1801743 (2018).

6 Clinckemalie, L. *et al.* Challenges and Opportunities for $CsPbBr_3$ Perovskites in Low- and High-Energy Radiation Detection. *ACS. Energy. Lett.* **6**, 1290-1314 (2021).

7 Zhou, Y., Chen, J., Bakr, O. M. & Mohammed, O. F. Metal Halide Perovskites for X-ray Imaging Scintillators and Detectors. *ACS. Energy. Lett.* **6**, 739-768 (2021).

8 Pan, W. *et al.* $Cs_2AgBiBr_6$ Single-Crystal X-Ray Detectors with a Low Detection Limit. *Nat. Photon.* **11**, 726-732 (2017).

9 Wei, H. *et al.* Sensitive X-ray Detectors Made of Methylammonium Lead Tribromide Perovskite Single Crystals. *Nat. Photon.* **10**, 333-339 (2016).

10 Xu, L. J., Lin, X., He, Q., Worku, M. & Ma, B. Highly Efficient Eco-Friendly X-ray Scintillators based on an Organic Manganese Halide. *Nat. Commun.* **11**, 4329 (2020).

11 Wei, J.-H. *et al.* All-Inorganic Lead-Free Heterometallic $Cs_4MnBi_2Cl_{12}$ Perovskite Single Crystal with Highly Efficient Orange Emission. *Matter.* **3**, 892-903 (2020).

12 Jana, A., Park, S., Cho, S., Kim, H. & Im, H. Bounce Back with Triplet Excitons for Efficient X-Ray Scintillation. *Matter.* **5**, 20-22 (2022).

13 Yang, B. *et al.* Lead-Free Halide Rb_2CuBr_3 as Sensitive X-Ray Scintillator. *Adv. Mater.* **31**, e1904711 (2019).

14 Han, K. *et al.* Seed Crystal Induced Cold Sintering Toward Metal Halide Transparent Ceramic Scintillators. *Adv. Mater.* **34**, e2110420 (2022).

15 Ma, W. *et al.* Thermally Activated Delayed Fluorescence (TADF) Organic Molecules for Efficient X-Ray Scintillation and Imaging. *Nat. Mater.* **21**, 210-216 (2022).

16 Wang, J.-X. *et al.* Nearly 100% Energy Transfer at the Interface of Metal-Organic Frameworks for X-Ray Imaging Scintillators. *Matter.* **5**, 253-265 (2022).

17 Gandini, M. *et al.* Efficient, Fast and Reabsorption-Free Perovskite Nanocrystal-based Sensitized Plastic Scintillators. *Nat. Nanotechnol.* **15**, 462-468 (2020).

18 Wang, X. *et al.* Color-Tunable X-ray Scintillation based on A Series of Isotypic Lanthanide-Organic Frameworks. *Chem. Commun.* **56**, 233-236 (2019).

19 Wang, X. *et al.* Organic Phosphors with Bright Triplet Excitons for Efficient X-Ray-Excited Luminescence. *Nat. Photon.* **15**, 187-192 (2021).

20 Galunov, N. *et al.* Delayed Radioluminescence of some Heterostructured Organic Scintillators. *J. Lumin.* **226**, 117477 (2020).

21 Wang, J. X. *et al.* Organic Thermometers Based on Aggregation of Difluoroboron beta-Diketonate Chromophores. *J. Phys. Chem. A.* **124**, 10082-10089 (2020).

22 Wang, X. F. *et al.* Pure Organic Room Temperature Phosphorescence from Excited Dimers in Self-Assembled Nanoparticles under Visible and Near-Infrared Irradiation in Water. *J. Am. Chem. Soc.* **141**, 5045-5050 (2019).

23 Zhang, X. *et al.* Ultralong Phosphorescence Cellulose with Excellent Anti-Bacterial, Water-Resistant and Ease-to-Process Performance. *Nat. Commun.* **13**, 1117 (2022).

24 Wang, J. X. *et al.* Tunable Fluorescence and Afterglow in Organic Crystals for Temperature Sensing. *J. Phys. Chem. Lett.* **13**, 1985-1990 (2022).

25 Dai, W. *et al.* Halogen Bonding: A New Platform for Achieving Multi-Stimuli-Responsive Persistent Phosphorescence. *Angew. Chem. Int. Ed.* **61**, e202200236 (2022).

26 Jeon, S. O. *et al.* High-Efficiency, Long-Lifetime Deep-Blue Organic Light-Emitting Diodes. *Nat. Photon.* **15**, 208-215 (2021).

27 Hirata, S. *et al.* Highly Efficient Blue Electroluminescence based on Thermally Activated Delayed Fluorescence. *Nat. Mater.* **14**, 330-336 (2015).

28 Yang, Z. *et al.* Recent Advances in Organic Thermally Activated Delayed Fluorescence Materials. *Chem. Soc. Rev.* **46**, 915-1016 (2017).

29 Wang, J.-X. *et al.* Organic Composite Crystal with Persistent Room-Temperature Luminescence Above 650 nm by Combining Triplet–Triplet Energy Transfer with Thermally Activated Delayed Fluorescence. *CCS. Chem.* **2**, 1391-1398 (2020).

30 Ding, D. *et al.* Highly Efficient and Color-Stable Thermally Activated Delayed Fluorescence White Light-Emitting Diodes Featured with Single-Doped Single Emissive Layers. *Adv. Mater.* **32**, e1906950 (2020).

31 Luo, D., Chen, Q., Gao, Y., Zhang, M. & Liu, B. Extremely Simplified, High-Performance, and Doping-Free White Organic Light-Emitting Diodes Based on a Single Thermally Activated Delayed Fluorescent Emitter. *ACS. Energy. Lett.* **3**, 1531-1538 (2018).

32 Tang, L. *et al.* X-ray Excited Ultralong Room-Temperature Phosphorescence for Organic Afterglow Scintillators. *Chem. Commun.* **56**, 13559-13562 (2020).

33 Dong, C. *et al.* Influence of Isomerism on Radioluminescence of Purely Organic Phosphorescence Scintillators. *Angew. Chem. Int. Ed.* **60**, 27195-27200 (2021).

34 Chen, H. *et al.* Cesium Lead Halide Nanocrystals based Flexible X-Ray Imaging Screen and Visible Dose Rate Indication on Paper Substrate. *Adv. Opt. Mater.* **10**, 2102790 (2022).

35 Han, L. *et al.* Photophysics in Zero-Dimensional Potassium-Doped Cesium Copper Chloride $Cs_3Cu_2Cl_5$ Nanosheets and Its Application for High-Performance Flexible X-Ray Detection. *Adv. Opt. Mater.* **10**, 2102453 (2022).

36 Liu, Y. *et al.* Large Lead-Free Perovskite Single Crystal for High-Performance Coplanar X-Ray Imaging Applications. *Adv. Opt. Mater.* **8**, 2000814 (2020).

37 Lian, L. *et al.* Highly Luminescent Zero-Dimensional Organic Copper Halides for X-ray Scintillation. *J. Phys. Chem. Lett.* **12**, 6919-6926 (2021).

38 Zhang, Y. *et al.* Metal Halide Perovskite Nanosheet for X-ray High-Resolution Scintillation Imaging Screens. *ACS. Nano.* **13**, 2520-2525 (2019).

39 Wang, J.-X. *et al.* Perovskite-Nanosheet Sensitizer for Highly Efficient Organic X-ray Imaging Scintillator. *ACS. Energy. Lett.* **7**, 10-16 (2021).

40 Kretzschmar, A., Patze, C., Schwaebel, S. T. & Bunz, U. H. Development of Thermally Activated Delayed Fluorescence Materials with Shortened Emissive Lifetimes. *J. Org. Chem.* **80**, 9126-9131 (2015).

41 Kim, H. S. *et al.* Enhancement of Reverse Intersystem Crossing in Charge-Transfer Molecule through Internal Heavy Atom Effect. *Adv. Funct. Mater.* **31**, 2104646 (2021).

42 Berger, M. J. et al. XCOM: Photon Cross Sections Database (National Institute of Standards and Technology, 2013); https://www.nist.gov/pml/xcom-photoncross-sections-database